Imposing a node at a desired location along a beam under harmonic base excitation: Theory and experiment

J. H. Porter[a], P. S. Harvey Jr.[b,*]

[a]*School of Aerospace and Mechanical Engineering, University of Oklahoma, Norman, OK 73019, USA*
[b]*School of Civil Engineering and Environmental Science, University of Oklahoma, Norman, OK 73019, USA*

Abstract

Vibration absorbers are commonly used to reduce unwanted structural vibrations. In this paper, a vibration absorber comprised of a sprung mass is used to enforce a location of zero displacement (or node) at a specified location on an Euler-Bernoulli beam under harmonic base excitation. Closed form expressions for the optimal tuning of the auxiliary spring-mass system are found, and results are presented for the cases of the attachment and node located at the same and different locations. The assumed modes method is used, so the results can be applied for arbitrary boundary conditions. To aid in the design process, this paper also characterizes the sensitivity of the displacement at the desired node location to parametric variations. Sensitivities are considered with respect to the base excitation frequency and the attachment mass, stiffness, and location. The sensitivities of the system highlight some feasible but less desirable attachment locations. Numerical and experimental results for a cantilever beam are presented to illustrate the proposed method and the effects of mistuning.

Keywords: node, constraint, vibration absorber, tuning, sensitivity

1. Introduction

1.1. Vibration absorbers

There is a rich history of research and literature on vibration absorbers dating back to seminal work by Frahm [1], Den Hartog [2], and Brock [3]. Applications of vibration absorbers have widely varied over the years, as have the design strategies [4, 5]. Many past studies have focused on single-degree-of-freedom (SDOF) primary systems to which a SDOF absorber is attached, but the focus of this paper is on enforcing

*Corresponding author.
Email address: harvey@ou.edu (P. S. Harvey Jr.)

nodes (i.e., locations of zero displacement) for base-excited beams whose dynamics cannot be captured with a single mode alone.

Extensive work has been performed on vibration absorbers for base-excited structures. For example, Warburton and Ayorinde [6] discuss how to find the optimum damper parameters for a simple system under support (base) excitation, Joshi and Jangid [7] considered using multiple tuned mass dampers to reduce the sensitivity to mistuning for a SDOF system undergoing white noise base excitation, and Tsai and Lin [8] found optimal parameters (based on the criteria of Den Hartog) for harmonic support excitation where the acceleration or displacement amplitude is fixed and independent of frequencies. However, all of these studies considered simply systems that could be modeled by a single normal mode.

Vibration absorbers have also been designed for continuous systems, such as beams [9] and plates [10], considering multiple modes of vibration. For example, Jacquot [11] considered vibration absorbers to eliminate large vibrations near a natural frequency of a beam. He used multiple attachments to reduce the effects of multiple modes resulting in a flattening of the frequency response. Dayou considered an attachment to a continuous system to minimize the kinetic energy of the beam and considered multiple forcing frequencies [12]. However, these examples and most other studies focus on point or distributed forcing applied to the structure, as opposed to base excitation.

1.2. Enforcing nodes

As previously noted, the focus of this paper is on the enforcement of nodes (or locations of zero displacement) along a beam under base excitation. There is a rich body of work by Cha and colleagues that considers using one or multiple attachments to enforce a node at a desired location on a beam for either free vibration or point forcing. These studies are summarized here.

Originally, Cha [13] proposed a method of enforcing nodes with absorbers at the same locations on the modified orthogonal modes of a continuous system (i.e., collocated). This methodology was developed for free vibration of beams, but he notes that it is applicable to forcing near one of the modified natural frequencies. He then considered creating single or multiple nodes with either collocated or not collocated attachments for a single forcing frequency [14]. The method was then expanded to include limitations on the maximum amplitudes of the attachments [15]. Cha and Rinker [16] later expanded the method to include damping of both the beam and the absorbers, as well as outlining an efficient numerical technique for solving for the system parameters.

Cha and Zhou [17] expanded the work to include enforcing both zero amplitude and zero slope at the

desired location by attaching both translational and rotational absorbers. This had the added benefit of a larger region of zero displacement. Cha and Chan [18] later updated this method to consider two degree of freedom attachments with two springs to act as both the rotational and translational absorbers.

Cha and Ren [19] considered harmonic excitation at multiple frequencies in their design of attachments to enforce nodes, which allowed them to create a frequency range with little to no displacement at the desired node location. Cha and Buyco [19] developed a more efficient method of solving for the system parameters for harmonic forcing at multiple frequencies; their proposed method solved for active forces and allowed for easy application of limitations on absorber amplitudes.

In all the above referenced studies, numerical experiments were used to demonstrate the various approaches, but no physical experiments have been reported. Wong et al. [20] experimentally validated an approach similar to that of Cha and Zhou [17] for enforcing fixed nodes (i.e., zero translation and rotation) with translational and rotational absorbers. Furthermore, Cha and colleagues have exclusively considered point force excitations. Rinker [21] previously investigated node enforcement for base excitation of a shear-type building, but she did not consider node enforcement of a continuous beam-type structure undergoing base excitation. Moreover, none of the previous work has considered analytical sensitivities to perturbations in the system parameters.

It is worth mentioning here the close relationship between imposing vibration nodes in a beam and the more general problem of response *localization* [22, 23]. The latter aims to localize the vibration modes to a small, but non-zero-measure, region of a beam [24, 25, 26] (or nominally periodic structure [23, 27, 28]), whereas the former seeks to suppress the vibrations at a point (i.e., zero-measure localization). Cha and Zhou [17] showed that, through proper tuning of sprung masses and rotational oscillators, nearly zero amplitudes could be imposed along a non-zero-measure region of a beam under localized harmonic loading.

In this paper, the theory for node enforcement on a beam under base excitation is developed. An approach similar to Cha's earlier work [14] is followed, with the addition of base excitation, as well as analytical parametric sensitivities and experimental demonstration. The case of only a single node and attachment is considered here, but the methods can easily be generalized to the case of multiple nodes and multiple attachments. However for the case of multiple noncollocated nodes and attachments, it is not possible to obtain a closed form solution. It should also be noted that the method developed in this paper can only be used to enforce a node at steady state.

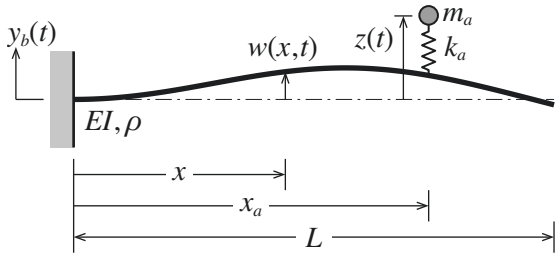

Figure 1: A cantilever beam subjected to a base excitation and carrying an attached sprung mass.

2. Theory

2.1. Governing Equations

Consider an elastic beam of length L undergoing base displacement $y_b(t)$, as shown in Fig. 1. The transverse deflection of the beam (relative to its base) is given by $w(x,t)$ for $0 \leqslant x \leqslant L$. A sprung mass (k_a, m_a) is attached at $x = x_a$, and its displacement (relative to the base) is given by $z(t)$. Without loss of generality, $z = 0$ is assumed to coincide with the static equilibrium position of the sprung mass. Modeling the uniform beam by the Euler–Bernoulli theory, the kinetic and potential energies of the system are respectively given by

$$T = \frac{1}{2}\int_0^L \rho(x)\,[\dot{w}(x,t) + \dot{y}_b(t)]^2\,dx + \frac{1}{2}m_a[\dot{z}(t) + \dot{y}_b(t)]^2 \tag{1a}$$

$$V = \frac{1}{2}\int_0^L EI(x)\,[w''(x,t)]^2\,dx + \frac{1}{2}k_a[z(t) - w(x_a,t)]^2 \tag{1b}$$

where EI and ρ are the flexural rigidity and length density of the beam, respectively.

Using a Rayleigh-Ritz approach, the transverse deflection can be expanded as follows:

$$w(x,t) = \boldsymbol{\phi}^T(x)\,\boldsymbol{\eta}(t) \equiv \sum_{i=1}^{N} \phi_i(x)\eta_i(t) \tag{2}$$

where $\boldsymbol{\phi}(x) = [\phi_1(x)\ \cdots\ \phi_N(x)]^T$ in which $\phi_i(x)$ are the eigenfunctions of the beam without the attachment, and $\boldsymbol{\eta}(t) = [\eta_1(t)\ \cdots\ \eta_N(t)]^T$ in which $\eta_i(t)$ are the corresponding generalize coordinates. Applying Lagrange's equation for $q \in \{\eta_1, \ldots, \eta_N, z\}$, the equations of motion for the beam–attachment system are

$$\mathbf{M}\ddot{\boldsymbol{\eta}}(t) + (\mathbf{K} + k_a\boldsymbol{\phi}_a\boldsymbol{\phi}_a^T)\boldsymbol{\eta}(t) - k_a\boldsymbol{\phi}_a z(t) = -\mathbf{m}_b\ddot{y}_b(t) \tag{3a}$$

$$m_a\ddot{z}(t) - k_a\boldsymbol{\phi}_a^T\boldsymbol{\eta}(t) + k_a z(t) = -m_a\ddot{y}_b(t) \tag{3b}$$

where $\boldsymbol{\phi}_a = [\phi_1(x_a)\ \cdots\ \phi_N(x_a)]^T$ and $\mathbf{m}_b = [m_b^{(1)}\ \cdots\ m_b^{(N)}]^T$ in which $m_b^{(i)} = \int_0^L \rho\phi_i(x)\,dx$. The $N \times N$ matrices $\mathbf{M}$ and $\mathbf{K}$ are diagonal matrices whose ith entries are the generalized mass M_i and stiffness K_i of

the beam alone:

$$M_i = \int_0^L \rho[\phi_i(x)]^2\,dx \quad \text{and} \quad K_i = \int_0^L EI[\phi_i''(x)]^2\,dx \tag{4}$$

Now, consider a harmonic base motion $y_b(t) = \mathrm{Re}[\overline{y}_b \exp(\mathrm{j}\omega t)]$, where $\overline{y}_b$ is the base displacement amplitude, ω is the excitation frequency, and $\mathrm{j} = \sqrt{-1}$. Assuming a harmonic response with the same frequency as the excitation frequency, i.e., $\boldsymbol{\eta}(t) = \mathrm{Re}[\overline{\boldsymbol{\eta}} \exp(\mathrm{j}\omega t)]$ and $z(t) = \mathrm{Re}[\overline{z} \exp(\mathrm{j}\omega t)]$, the following compact matrix equation is obtained:

$$\begin{bmatrix} \mathbf{K} - \omega^2\mathbf{M} + k_a\boldsymbol{\phi}_a\boldsymbol{\phi}_a^T & -k_a\boldsymbol{\phi}_a \\ -k_a\boldsymbol{\phi}_a^T & k_a - \omega^2 m_a \end{bmatrix} \begin{Bmatrix} \overline{\boldsymbol{\eta}} \\ \overline{z} \end{Bmatrix} = \omega^2 \overline{y}_b \begin{Bmatrix} \mathbf{m}_b \\ m_a \end{Bmatrix} \tag{5}$$

Finding $\overline{z}$ (in terms of $\overline{\boldsymbol{\eta}}$) from the lower block equation,

$$\overline{z} = \frac{k_a\boldsymbol{\phi}_a^T\overline{\boldsymbol{\eta}} + \omega^2\overline{y}_b m_a}{k_a - \omega^2 m_a} \tag{6}$$

and substituting this expression into the upper block equations gives

$$\overline{\boldsymbol{\eta}} = [\mathbf{K} - \omega^2\mathbf{M} + \sigma\boldsymbol{\phi}_a\boldsymbol{\phi}_a^T]^{-1}(\omega^2\mathbf{m}_b - \sigma\boldsymbol{\phi}_a)\overline{y}_b \tag{7}$$

where

$$\sigma \doteq \frac{m_a k_a \omega^2}{\omega^2 m_a - k_a} \tag{8}$$

The inverse of the term in brackets can be found to be

$$[\mathbf{K} - \omega^2\mathbf{M} + \sigma\boldsymbol{\phi}_a\boldsymbol{\phi}_a^T]^{-1} = (\mathbf{K} - \omega^2\mathbf{M})^{-1} - \frac{\sigma}{1 + \boldsymbol{\phi}_a^T(\mathbf{K} - \omega^2\mathbf{M})^{-1}\boldsymbol{\phi}_a\,\sigma}(\mathbf{K} - \omega^2\mathbf{M})^{-1}\boldsymbol{\phi}_a\boldsymbol{\phi}_a^T(\mathbf{K} - \omega^2\mathbf{M})^{-1} \tag{9}$$

using the Sherman–Morrison formula.

2.2. Tuning the attachment

The total displacement (relative to an inertial reference frame) along the beam is denoted

$$y(x,t) = w(x,t) + y_b(t), \tag{10}$$

and the displacement amplitude at a point along the beam is given by

$$\overline{y}(x) = \boldsymbol{\phi}^T(x)\,\overline{\boldsymbol{\eta}} + \overline{y}_b \tag{11}$$

To impose a node at $x = x_n$ requires that

$$y(x_n,t) = 0, \forall t \Rightarrow \overline{y}_n \equiv \boldsymbol{\phi}_n^T\overline{\boldsymbol{\eta}} + \overline{y}_b = 0 \tag{12}$$

where $\overline{y}_n = \overline{y}(x_n)$ and $\boldsymbol{\phi}_n = [\phi_1(x_n) \ \cdots \ \phi_N(x_n)]^T$. Substituting the expression for $\overline{\boldsymbol{\eta}}$ from Eq. (7) into this constraint gives

$$\omega^2 \boldsymbol{\phi}_n^T (\mathbf{K} - \omega^2 \mathbf{M})^{-1} \mathbf{m}_b - \frac{\boldsymbol{\phi}_n^T (\mathbf{K} - \omega^2 \mathbf{M})^{-1} \boldsymbol{\phi}_a \boldsymbol{\phi}_a^T (\mathbf{K} - \omega^2 \mathbf{M})^{-1} \mathbf{m}_b \omega^2 \sigma}{1 + \boldsymbol{\phi}_a^T (\mathbf{K} - \omega^2 \mathbf{M})^{-1} \boldsymbol{\phi}_a \sigma}$$
$$- \boldsymbol{\phi}_n^T (\mathbf{K} - \omega^2 \mathbf{M})^{-1} \boldsymbol{\phi}_a \sigma + \frac{\boldsymbol{\phi}_n^T (\mathbf{K} - \omega^2 \mathbf{M})^{-1} \boldsymbol{\phi}_a \boldsymbol{\phi}_a^T (\mathbf{K} - \omega^2 \mathbf{M})^{-1} \boldsymbol{\phi}_a \sigma^2}{1 + \boldsymbol{\phi}_a^T (\mathbf{K} - \omega^2 \mathbf{M})^{-1} \boldsymbol{\phi}_a \sigma} + 1 = 0 \quad (13)$$

Solving for σ, the (unique) root is

$$\sigma = \frac{1 + c_{nb} \omega^2}{c_{na} c_{ab} \omega^2 - c_{aa} c_{nb} \omega^2 + c_{na} - c_{aa}} \quad (14)$$

where

$$c_{na} \doteq \boldsymbol{\phi}_n^T (\mathbf{K} - \omega^2 \mathbf{M})^{-1} \boldsymbol{\phi}_a \equiv \sum_{i=1}^{N} \frac{\phi_i(x_n) \phi_i(x_a)}{K_i - \omega^2 M_i} \quad (15a)$$

$$c_{nb} \doteq \boldsymbol{\phi}_n^T (\mathbf{K} - \omega^2 \mathbf{M})^{-1} \mathbf{m}_b \equiv \sum_{i=1}^{N} \frac{\phi_i(x_n) \, m_b^{(i)}}{K_i - \omega^2 M_i} \quad (15b)$$

$$c_{aa} \doteq \boldsymbol{\phi}_a^T (\mathbf{K} - \omega^2 \mathbf{M})^{-1} \boldsymbol{\phi}_a \equiv \sum_{i=1}^{N} \frac{\phi_i^2(x_a)}{K_i - \omega^2 M_i} \quad (15c)$$

$$c_{ab} \doteq \boldsymbol{\phi}_a^T (\mathbf{K} - \omega^2 \mathbf{M})^{-1} \mathbf{m}_b \equiv \sum_{i=1}^{N} \frac{\phi_i(x_a) \, m_b^{(i)}}{K_i - \omega^2 M_i} \quad (15d)$$

Assuming either the attachment stiffness k_a or the attachment mass m_a is specified (as well as the base excitation frequency ω, the desired node location x_n, and the attachment location x_a), a closed form expression for the required m_a or k_a, respectively, can be obtained from Eq. (8):

$$m_a(\omega, x_n, x_a, k_a) = \frac{k_a \sigma}{\omega^2 \sigma - k_a \omega^2} \quad \text{or} \quad k_a(\omega, x_n, x_a, m_a) = \frac{m_a \omega^2 \sigma}{m_a \omega^2 + \sigma} \quad (16)$$

where $\sigma \equiv \sigma(\omega, x_n, x_a)$ is given by Eq. (14).

Collocated case. For the case where the attachment and node locations are collocated (i.e., $x_n = x_a$), the denominator in Eq. (14) goes to zero because $\boldsymbol{\phi}_a = \boldsymbol{\phi}_n$, so σ goes to ∞. Taking the limit of Eq. (16) as $\sigma \to \infty$, the attachment mass and stiffness would need to be tuned to the excitation frequency ω, i.e.

$$m_a = k_a / \omega^2 \text{ or } k_a = \omega^2 m_a \quad (17)$$

This result is consistent with Cha [14] for the point loaded beam.

Limitations. It is worth noting that Eqs. (16) and (17) were derived under the assumption that the transient (homogeneous) solution can be ignored, which is not strictly correct for undamped systems, but is classically assumed for convenience [2]. The response of a damped system is ultimately governed by its steady-state (particular) solution, which for arbitrarily small damping is not dissimilar to that of an undamped system. Therefore, the tuned masses and stiffnesses given in Eqs. (16) and (17) may nearly enforce a node for very lightly damped systems (as shown in Sec. 4), but care should nevertheless be taken when extrapolating these results for damped systems. Future studies should consider the incorporation of damping and its effect on the attachment tuning.

2.3. Sensitivity analysis

In this section, the sensitivity of the beam's response to mistuning is analyzed. In particular, the quantity of interest being investigated is the amplitude of the total displacement of the beam at the desired node location:

$$\bar{y}_n = \boldsymbol{\phi}_n^T \bar{\boldsymbol{\eta}} + \bar{y}_b \tag{18}$$

The variables of interest are the mass m_a, stiffness k_a, and location x_a of the attachment, as well as the base excitation frequency ω; i.e., $\bar{y}_n \equiv \bar{y}_n(m_a, k_a, x_a, \omega)$.

For the perfectly tuned variables (denoted m_a^*, k_a^*, x_a^*, and ω^*), the deflection is zero by construction:

$$\bar{y}_n(m_a^*, k_a^*, x_a^*, \omega^*) = 0$$

The variation of $\bar{y}_n$ to small perturbations in m_a, k_a, x_a, and ω about the tuned condition is given by

$$\delta\bar{y}_n = \bar{y}_n(m_a^* + \delta m_a, k_a^* + \delta k_a, x_a^* + \delta x_a, \omega^* + \delta\omega) - \bar{y}_n(m_a^*, k_a^*, x_a^*, \omega^*) \tag{19}$$

$$= \left(\frac{\partial \bar{y}_n}{\partial m_a}\right)^* \delta m_a + \left(\frac{\partial \bar{y}_n}{\partial k_a}\right)^* \delta k_a + \left(\frac{\partial \bar{y}_n}{\partial x_a}\right)^* \delta x_a + \left(\frac{\partial \bar{y}_n}{\partial \omega}\right)^* \delta\omega + \text{h.o.t.} \tag{20}$$

where $(\cdot)^* = (\cdot)|_{(m_a^*, k_a^*, x_a^*, \omega^*)}$. From this equation, the sensitivity of $\bar{y}_n$ with respect to a given variable is found from the first derivative of $\bar{y}_n$ with respect to that variable evaluated at $(m_a^*, k_a^*, x_a^*, \omega^*)$. From Eq. (18), the partial derivatives are found to be

$$\frac{\partial \bar{y}_n}{\partial p} = \boldsymbol{\phi}_n^T \frac{\partial \bar{\boldsymbol{\eta}}}{\partial p} + \frac{\partial \bar{y}_b}{\partial p}, \quad p \in \{m_a, k_a, x_a, \omega\} \tag{21}$$

To determine the sensitivity with respect to a given variable, the partial derivatives $\partial\bar{\boldsymbol{\eta}}/\partial p$ and $\partial\bar{y}_b/\partial p$ need to be evaluated. Note that the latter is always zero for $p = m_a$, k_a, and x_a:

$$\partial\bar{y}_b/\partial m_a = \partial\bar{y}_b/\partial k_a = \partial\bar{y}_b/\partial x_a = 0 \tag{22}$$

However, the derivative $\partial\overline{y}_b/\partial\omega$ depends on whether the displacement amplitude $\overline{y}_b$ or acceleration amplitude $\ddot{\overline{y}}_b$ ($= -\omega^2\overline{y}_b$) of the base is held constant:

$$\partial\overline{y}_b/\partial\omega = \begin{cases} 0, & \overline{y}_b \text{ constant} \\ 2\ddot{\overline{y}}_b/\omega^3, & \ddot{\overline{y}}_b \text{ constant} \end{cases} \tag{23}$$

The latter case will be considered hereinafter because it corresponds to the experiments.

To determine the partial derivatives $\partial\overline{\boldsymbol{\eta}}/\partial p$, the matrix equation (5) is differentiated with respect to each variable, which after re-arranging terms can be written as follows:

$$\mathbf{A}\begin{Bmatrix} \partial\overline{\boldsymbol{\eta}}/\partial p \\ \partial\overline{z}/\partial p \end{Bmatrix} = \frac{\partial}{\partial p}\left(-\ddot{\overline{y}}_b \begin{Bmatrix} \mathbf{m}_b \\ m_a \end{Bmatrix}\right) - \frac{\partial\mathbf{A}}{\partial p}\begin{Bmatrix} \overline{\boldsymbol{\eta}} \\ \overline{z} \end{Bmatrix}, \quad p \in \{m_a, k_a, x_a, \omega\} \tag{24}$$

where $\mathbf{A}$ is the system matrix in Eq. (5). Evaluating the derivatives on the right hand side of this equation for each variable, the derivatives appearing on the left side are solved for:

$$\begin{Bmatrix} \partial\overline{\boldsymbol{\eta}}/\partial p \\ \partial\overline{z}/\partial p \end{Bmatrix} = \mathbf{A}^{-1}\begin{cases} \begin{Bmatrix} \mathbf{0} \\ -\ddot{\overline{y}}_b + \omega^2\overline{z} \end{Bmatrix}, & p = m_a \\ \begin{Bmatrix} -\boldsymbol{\phi}_a\boldsymbol{\phi}_a^T\overline{\boldsymbol{\eta}} + \boldsymbol{\phi}_a\overline{z} \\ \boldsymbol{\phi}_a^T\overline{\boldsymbol{\eta}} - \overline{z} \end{Bmatrix}, & p = k_a \\ \begin{Bmatrix} -k_a(\boldsymbol{\phi}_a'\boldsymbol{\phi}_a^T + \boldsymbol{\phi}_a\boldsymbol{\phi}_a'^T)\overline{\boldsymbol{\eta}} + k_a\boldsymbol{\phi}_a'\overline{z} \\ k_a\boldsymbol{\phi}_a'^T\overline{\boldsymbol{\eta}} \end{Bmatrix}, & p = x_a \\ \begin{Bmatrix} 2\omega\mathbf{M}\overline{\boldsymbol{\eta}} \\ 2\omega m_a\overline{z} \end{Bmatrix}, & p = \omega \end{cases} \tag{25}$$

where $\boldsymbol{\phi}_a' = [\phi_1'(x_a) \ \cdots \ \phi_N'(x_a)]^T$.

Finally, to determine the local sensitivity, Eqs. (22), (23), and (25) are evaluated at $m_a = m_a^*$, $k_a = k_a^*$, $x_a = x_a^*$, and $\omega = \omega^*$, and then substituted into Eq. (21). The calculated sensitivities can be used to evaluate the robustness of the absorber to slight mistuning, which is important in designing such an absorber. In Sec. 3.1, these sensitivities are calculated for two example design scenarios.

3. Numerical Results

Because the assumed modes method (Rayleigh-Ritz) was used in formulating the equations of motion, the development in the previous section is applicable for any arbitrarily supported elastic structure during

harmonic base excitation, so long as a uniform base excitation is applied at all supports. Without loss of generality, a cantilever (fixed-free) beam with uniform properties (EI, ρ) is considered in this section. The mass-normalized assumed mode shapes for a cantilever beam were used:

$$\phi_i(x) = \frac{1}{\sqrt{\rho L}}\left(\cos\beta_i x - \cosh\beta_i x + \frac{\sin\beta_i L - \sinh\beta_i L}{\cos\beta_i L + \cosh\beta_i L}(\sin\beta_i x - \sinh\beta_i x)\right) \tag{26}$$

where the $\beta_i L$ are found from the transcendental equation

$$\cos\beta_i L \cosh\beta_i L = -1 \tag{27}$$

These give generalized mass and stiffness values of

$$M_i = 1 \text{ and } K_i = (\beta_i L)^4 EI/(\rho L^4) \tag{28}$$

The generalized inertial masses for these assumed mode shapes are

$$m_b^{(i)} = \sqrt{\frac{\rho}{L}}\frac{2(\sin\beta_i L - \sinh\beta_i L)}{\beta_i(\cos\beta_i L + \cosh\beta_i L)} \tag{29}$$

In the following numerical example, $N = 15$ modes are retained in the assumed-modes expansion (Eq. (2)), which is sufficient to ensure convergence in the numerical results [14].

The proposed approach is illustrated by imposing a node during harmonic base excitation at a frequency of $\omega = 31\sqrt{EI/(\rho L^4)}$ [14]. This base excitation frequency is between the second and third natural frequencies of the beam without an attachment, i.e., $4.694^2\sqrt{EI/(\rho L^4)}$ and $7.855^2\sqrt{EI/(\rho L^4)}$, respectively. It is desired to enforce a node at the tip of the beam (i.e., $x_n = 1.0L$) by incorporating an attachment with stiffness $k_a = 20EI/L^3$. Two cases are considered: attachment and node locations are (a) collocated and (b) not collocated. Fig. 2 shows the steady-state deflection amplitudes for both these cases. For the collocated cases, the attachment is tuned to the base excitation frequency per Eq. (17), i.e., $m_a = k_a/\omega^2 = 20\rho L/31^2$. For the non-collocated case, the attachment mass was calculated to be $m_a = 2.153\times10^{-2}\rho L$. For both cases, the addition of the attachment allows the tip of the beam to be "fixed" without applying any rigid support at the tip of the beam. Table 1 gives the sensitivities of the steady-state displacement amplitude $\bar{y}_n$ at the desired node location $x_n = 1.0L$ to the design parameters (m_a, k_a, x_a, and ω) for both these cases. The normalized sensitivities given in Table 1 are

$$s_{m_a} = \frac{\rho L}{\ddot{\bar{y}}_b/\omega^2}\frac{\partial\bar{y}_n}{\partial m_a}, \quad s_{k_a} = \frac{k_a}{\ddot{\bar{y}}_b/\omega^2}\frac{\partial\bar{y}_n}{\partial k_a}, \quad s_{x_a} = \frac{L}{\ddot{\bar{y}}_b/\omega^2}\frac{\partial\bar{y}_n}{\partial x_a}, \quad s_\omega = \frac{\omega}{\ddot{\bar{y}}_b/\omega^2}\frac{\partial\bar{y}_n}{\partial\omega} \tag{30}$$

where the partial derivatives $\partial\bar{y}_n/\partial(\cdot)$ are given in Eq. (21), which are evaluated at the tuned configuration $(m_a^*, k_a^*, x_a^*, \omega^*)$ under consideration. From the tabulated sensitivities, it is observed that the noncolocated

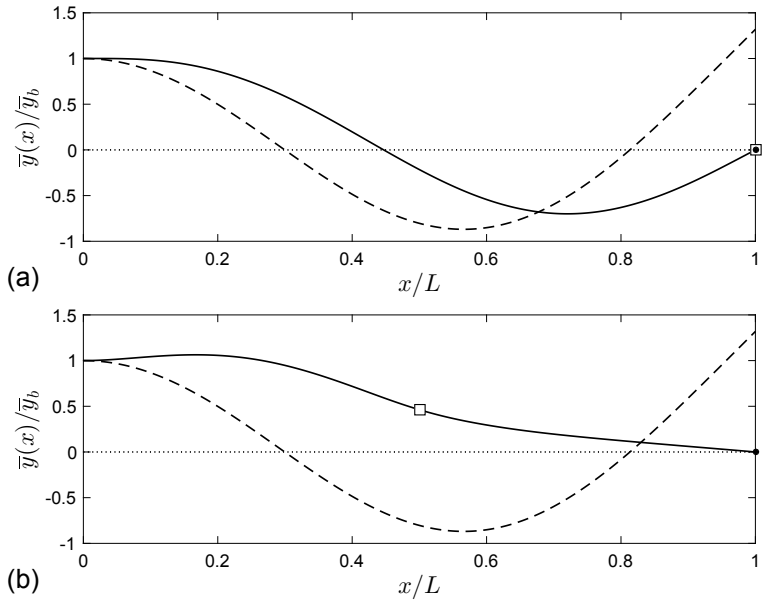

Figure 2: Steady-state deflection amplitudes of a uniform cantilever beam, without (− − −) and with (—) an attachment with stiffness $k_a = 20EI/L^3$, subject to base excitation with frequency $\omega = 31\sqrt{EI/(\rho L^4)}$. The attachment location (□) and node location (•) are: (a) collocated, $x_a = x_n = 1.0L$; (b) not collocated, $x_a = 0.5L$ and $x_n = 1.0L$.

case ($x_a = 0.5L$) is more sensitive than the collocated case ($x_a = 1.0L$) for all parameters except for attachment location x_a.

3.1. Feasible designs and their sensitivities

For the collocated case ($x_a = x_n$), it is always possible to design a feasible[1] attachment per Eq. (17) to create a node at an arbitrary point x_n. For the non-collocated cases ($x_a \neq x_n$), feasible attachment designs are not always possible. For example, Eq. (16) may require a negative mass or stiffness to achieve the node given the selected x_a and x_n.

[1]The design is not necessarily practical, e.g., a very large or very small mass or stiffness.

Table 1: Normalized sensitivities of the steady-state displacement amplitude $\overline{y}_n$ with respect to the attachment mass m_a, stiffness k_a, and location x_a, as well as base excitation frequency ω, for the two examples of Fig. 2.

x_a/L	s_{m_a}	s_{k_a}	s_{x_a}	s_ω
1.0	−295.4	6.148	−3.871	−12.30
0.5	−1016	22.64	0.3202	−45.12

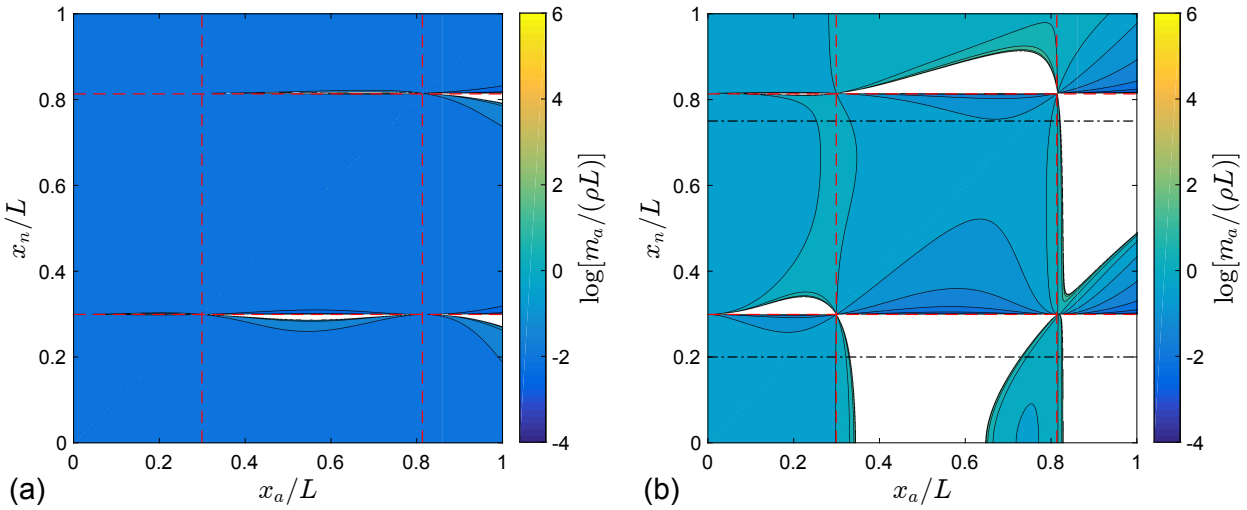

Figure 3: Attachment design maps for a uniform cantilever beam subject to base excitation with frequency $\omega = 31\sqrt{EI/(\rho L^4)}$. The charts depict the tuned attachment mass m_a per Eq. (16) for an attachment with k_a = (a) $20EI/L^3$ and (b) $400EI/L^3$ under varying attachment location x_a and node location x_n. The unshaded regions are infeasible, requiring a negative mass. The dashed lines correspond to the node locations for the cantilever without an attachment, and the dash-dotted lines correspond to the cases considered in Fig. 4.

Fig. 3 shows the required attachment mass m_a based on Eq. (16) and its dependence on possible node location x_n and attachment location x_a for a base excitation frequency of $\omega = 31\sqrt{EI/(\rho L^4)}$ and attachment stiffnesses of $k_a = 20EI/L^3$ and $400EI/L^3$. The colored regions are where it is possible to create a node at x_n by placing an attachment at x_a, whereas the unshaded areas require negative mass and therefore are not feasible. Closely spaced contours indicate regions where the required mass is sensitive to x_a and x_n. The highly sensitive regions tend to align with the node locations for the beam without attachments ($x/L = 0.30$ and 0.81) indicated by the dashed lines. For the considered base excitation frequency, the higher attachment stiffness (Fig. 3(b)) results in fewer feasible combinations of attachment and node locations. However, in some cases, a higher stiffness may be required to limit the amplitudes of the attachments thus restricting the possible attachment locations for a given node location.

To better visualize the dependence of the attachment mass m_a on attachment location x_a, Fig. 4 shows m_a versus x_a for two given node locations: x_n = (a) $0.75L$ and (b) $0.2L$, which correspond to the horizontal dash-dotted lines in Fig. 3(b). For both design plots, positive values of m_a indicate that a design is feasible while negative values indicate that it is not possible to create a node at the desired location given the specified attachment location.

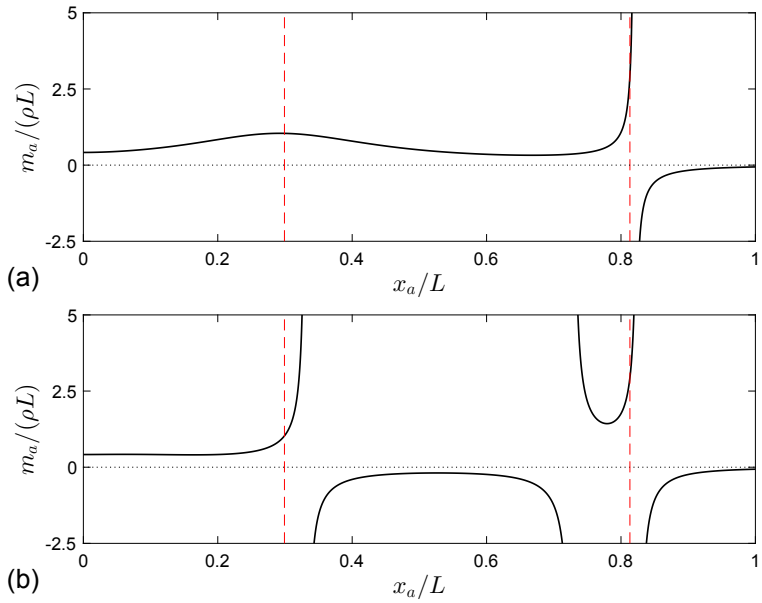

Figure 4: Required attachment mass m_a to enforce a node at x_n = (a) $0.75L$ and (b) $0.2L$ on a uniform cantilever beam subject to base excitation with frequency $\omega = 31\sqrt{EI/(\rho L^4)}$, for an attachment stiffness $k_a = 400EI/L^3$ and varying attachment location x_a. The dashed lines correspond to the node locations for the cantilever without an attachment.

Figs. 5 and 6 show the associated normalized sensitivities (Eq. (30)) of the steady-state displacement amplitudes at the desired node locations $x_n = 0.75L$ and $0.2L$, respectively, to the design parameters (m_a, k_a, x_a, and ω). The vertical lines in each figure represent the node locations for the unconstrained system. While for the given examples, they line up closely with the sensitivities diverging to infinite, this is not always the case.

For both cases, it is generally desired to minimize the sensitivity of the node displacement to the parameters to ensure that the effects of mistuning are minimized. However, depending on the system, the relative importance of each of the sensitivities may change.

For the node placed at $0.75L$ (Fig. 4(a)), it is possible to place the attachment anywhere on the beam closer to the base than $0.8L$ (see negative mass in Fig. 4(a)). For the considered case, the attachment masses (m_a) are all on the same order of magnitude as the beam mass (ρL). However, some locations do have smaller mass values. Some of the possible attachment locations are not desirable however because of large sensitivities to mistuning of parameters (see Fig. 5). For this case, the sensitivities diverge to infinity close to the base and the node locations of the unconstrained system. Therefore, the best designs to constrain the system would be to place the attachment between $0.1L$ to $0.25L$ or $0.35L$ to $0.7L$.

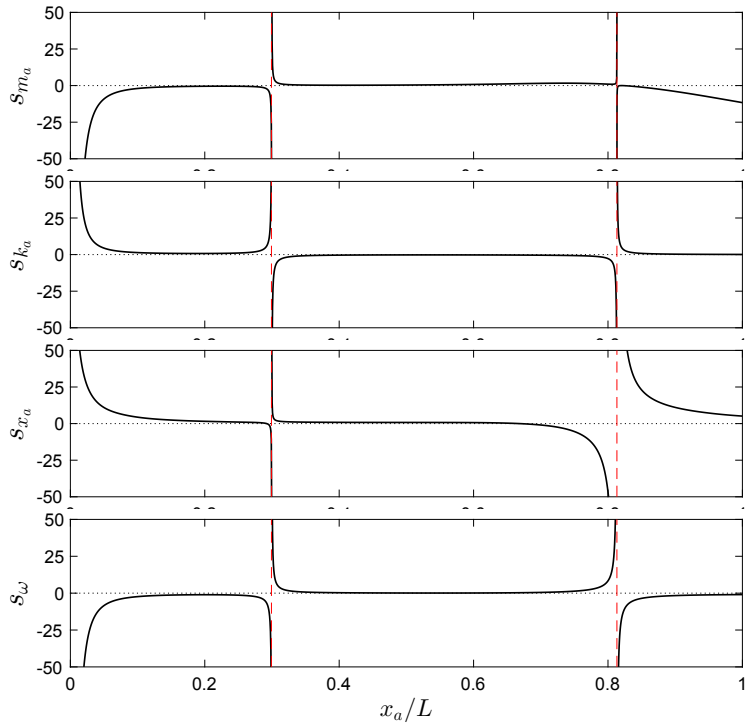

Figure 5: Normalized sensitivities of the steady-state total displacement amplitude $\bar{y}_n$ with respect to attachment mass m_a, stiffness k_a, and location x_a, as well as base excitation frequency ω, to enforce a node at $x_n = 0.75L$ on a uniform cantilever beam subject to ground excitation with frequency $\omega = 31\sqrt{EI/(\rho L^4)}$, for an attachment stiffness $k_a = 400EI/L^3$ and varying attachment location x_a.

For the node placed at $0.2L$ (Fig. 4(b)), the sensitivities are more interesting and do not line up as closely with the nodes of the unconstrained system. Based on Fig. 4(b), it is feasible to place the attachment from the base to $0.33L$ or from $0.74L$ to $0.82L$ because the mass values are positive. Based solely on the mass values, it may be undesirable to place the attachment near $0.8L$ because of the larger required mass ($> \rho L$). Based on the sensitivities of the system, the desirable locations can be further reduced. Of the feasible locations, near $0.75L$ the system shows some of the lowest sensitivities. However, if a smaller attachment mass is desired for the given spring stiffness, the region of less than $0.33L$ must be used. In that region, the smallest sensitivities are around $0.1L$. If the sensitivity to the attachment location is the most important, it is possible in both regions of feasible attachment locations to achieve a zero sensitivity to attachment location at the cost of higher sensitivities to other variables.

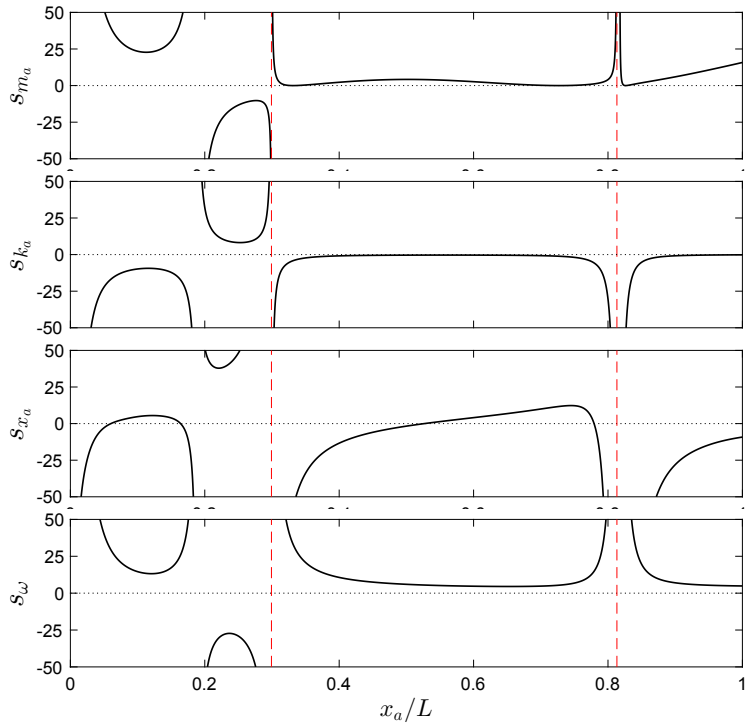

Figure 6: Normalized sensitivities of the steady-state total displacement amplitude $\bar{y}_n$ with respect to attachment mass m_a, stiffness k_a, and location x_a, as well as base excitation frequency ω, to enforce a node at $x_n = 0.2L$ on a uniform cantilever beam subject to ground excitation with frequency $\omega = 31\sqrt{EI/(\rho L^4)}$, for an attachment stiffness $k_a = 400EI/L^3$ and varying attachment location x_a.

4. Experiments

4.1. Experimental Setup

For the experiments, an aluminum yardstick was used as a flexible beam. The clamped and free lengths of the beam were 25.4 and 889 mm, respectively. The total mass of the beam was 151.3 g. The length density ρ of the beam was calculated by dividing the measured mass by the total length (914.4 mm).

The stiffness of the beam was extracted based on free vibration tests using a laser (ILD1302-200, Micro Epsilon, Ortenburg, Germany) to measure the position of the beam at 750 samples per second. The first three natural frequencies were extracted from the tests and the resulting values of EI calculated. The first three modes were lightly damped so the measured frequencies were not significantly impacted by damping. The first three natural frequencies were 1.84, 11.6, and 32.6 Hz. These resulted in estimates of flexural rigidity EI of 1.12, 1.14, and 1.14 $\mathrm{N\,m^2}$, respectively. The flexural rigidity determined from the second mode was used throughout this section because it is closest to the considered base excitation frequency and

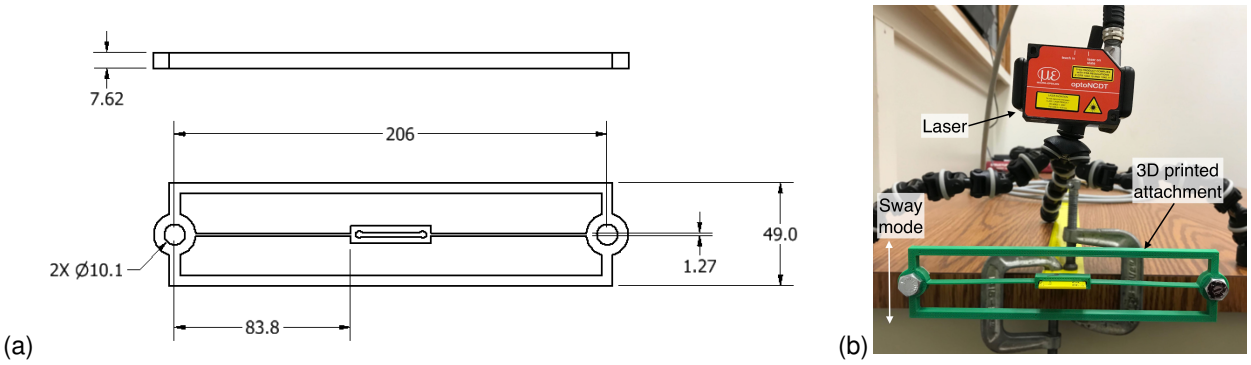

Figure 7: (a) Attachment drawing (units: mm); (b) setup to measure the natural frequency of the 3D printed attachment.

consistent with the flexural rigidity of the third mode (only 0.26% different).

A 3D printed attachment was designed to act as a vibration absorber, targeting a base excitation frequency of 9.5 Hz. Note that this frequency corresponds to $\omega \approx 17\sqrt{EI/(\rho L^4)}$, which is different than the case considered in Sec. 3. An effectively rigid rectangular box was connected to the aluminum beam by two very flexible beams attached to the press fit center. The total mass including the press fit center of the 3D printed portion (see Fig. 7(a)) was 22.0 g. For additional mass, two bolts and nuts were fastened to the box, one at either end. The total mass of the attachment with the two nuts and bolts was 67.4 g. The natural frequency of the attachment was extracted using the laser (see Fig. 7(b)). This gave a natural frequency of 15.9 Hz and therefore a calculated stiffness of $k_a = 673$ N/m using the total attachment mass. Note that, although the attachment was designed as a SDOF oscillator in sway, two torsional modes (roll and yaw) were also present, but these modes were designed to minimize their influence on the response for the experimental scenario considered. In particular, the roll mode (20.7 Hz), which corresponds to weak-axis bending in the beam, was tuned to have a high enough frequency to minimize its response at the nominal base excitation frequencies (9.5 Hz), and the yaw mode (8.08 Hz), which corresponds to torsion in the beam, has negligible influence on the bending modes of the beam.

The tests were conduced on a shake table (APS 113 ELECTRO-SEIS, APS Dynamics, San Juan Capistrano, CA, USA) shown in Fig. 8. The base excitation frequency was controlled with LabVIEW, and a constant amplitude of $0.6g$ was targeted. The table's acceleration was measured with an accelerometer (393B04, PCB, Depew, NY, USA), and the peak value of a fast Fourier transform (FFT) of the data was used to determine the table acceleration amplitude. The laser was again used to measure absolute beam displacements relative to the fixed ground.

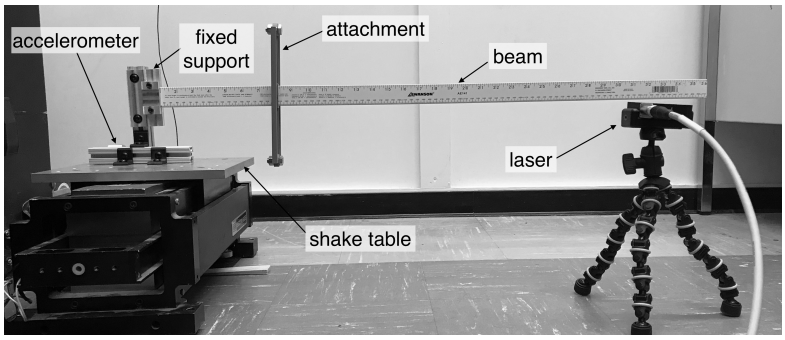

Figure 8: Experimental setup for test of base-excited beam with attachment.

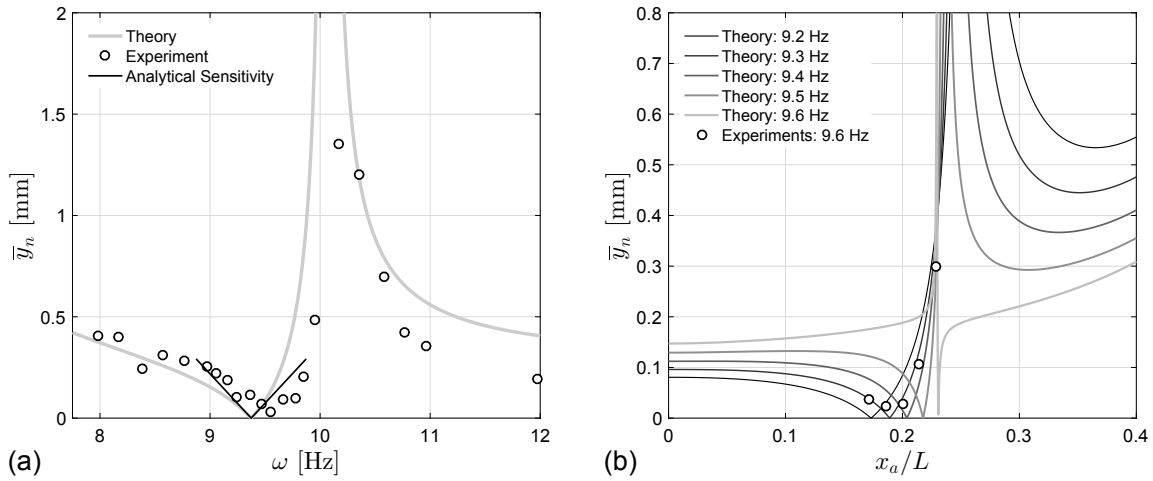

Figure 9: Comparison of theoretical and experimental displacement amplitude at the desired node location for varying (a) base excitation frequency ω and (b) attachment location x_a.

4.2. Experimental Results

Fig. 9 shows experimental data and the associated theoretical results. Two sets of tests were conducted to evaluate the sensitivity of the system to mistuning in the base excitation frequency ω and the attachment location x_a. Each of the theoretical results in Fig. 9 diverges to infinite corresponding to the attachment location that causes the modified system to have a natural frequency equal to the base excitation frequency. Though the theoretical curves in Fig. 9(a) and Fig. 9(b) appear similar, the curves cannot be directly compared because they are produced by varying different quantities (x_a and ω, respectively). These two cases are discussed here.

The first set of tests (Fig. 9(a)) illustrated the sensitivity of the system to mistuning of the base excitation frequency ω. For this test the attachment was placed 177.8 mm from the base ($x_a/L = 0.2$) and the laser

measured the displacements at the desired node location of 673.1 mm from the base ($x_n/L = 0.757$). The base excitation frequency was then varied while maintaining a constant base acceleration of $0.6g$. The theory line in Fig. 9(a) corresponds to the characterized parameters of the system and the chosen values of x_a and x_n. The analytical sensitivity corresponds to the local slope at the theoretical node found from Eq. (25). For the experimental data, the displacement was calculated based on selecting the peak in an FFT closest to the base excitation frequency. These amplitudes are plotted against the frequency of the associated peaks.

Fig. 9(a) shows acceptable agreement between the theory and experimental results for varying the base excitation frequency. The theoretical node based on the characterized system occurs at 9.37 Hz. In the experiment, the minimum displacement occurred at a system frequency of 9.55 Hz. This discrepancy could be due to damping or imperfect characterization of the system parameters. The experimental data, however, does closely follow the same shape as the expected results based on the characterized system. The experimental points in the range of 9.8 to 10.4 Hz are also generally located beneath the theoretical curve. This occurs because the real system has damping, so the response does not diverge near resonance like the theoretical system.

The second set of tests (Fig. 9(b)) illustrated the changes in the system with varying the attachment location x_a. Each theoretical line corresponds to the behavior of the characterized system when the attachment location is varied while at fixed base excitation frequency and acceleration. Multiple theory lines are plotted to illustrate how the behavior changes with the base excitation frequency. Qualitatively similar behavior is observed for forcing frequencies of 9.2 to 9.5 Hz, but between forcing frequencies of 9.5 and 9.6 Hz the node changes which side of resonance that it occurs on. The response at x_n is highly sensitive to frequency variations in this region.

For the experiments, the base excitation frequency was fixed at 9.6 Hz with a constant base acceleration of $0.6g$. The attachment was positioned at 152.4, 165.1, 177.8, 190.5, and 203.2 mm from the base ($x_a/L =$ 0.171, 0.186, 0.2, 0.214, and 0.229). For all of these tests, the laser measured the displacements at the desired node location of 673.1 mm from the base ($x_n/L = 0.757$). The peaks from the displacement FFT were again used to determine the amplitude of the response at the base excitation frequency. The second set of tests showed similar behavior to the theoretical line drawn at 9.3 Hz. The experimental data does not follow the same general shape of the theoretical line at 9.6 Hz because the system behavior is highly sensitive to the base excitation frequency as discussed above. The discrepancy between the theoretical and

experimental results likely is due to inaccuracy in the characterization of the initial system. Nevertheless, the experiments demonstrated the concept of enforcing nodes on a base-excited beam and the sensitivity to parametric variation.

5. Conclusion

This paper has expanded previously developed theory for enforcing nodes [14] to incorporate base excitation of continuous systems. Closed form expressions for the optimal tuning of an auxiliary spring-mass system are derived for the cases of the attachment and node located at the same and different locations. The procedure presented uses the assumed modes method, so it can be directly applied to arbitrary beam boundary conditions and nonuniform cross sections if the mode shapes can be found. In addition, analytical sensitivities of the combined system were derived to understand the effects of mistuning. In the future, these sensitivities could be applied to determine the optimal attachment location to create a given node in the presence of uncertainty.

Two numerical examples were presented to illustrate the value of the proposed method for enforcing a node on base-excited cantilever beams. Using the derived methods for determining the attachment mass and the sensitivity of the system, a number of design plots were created. These illustrated not only the required mass to achieve the node for a perfect system, but also the sensitivity of the system to mistuning. Some attachment locations were not possible because they required a negative mass. Other attachment locations result in a highly sensitive system making them undesirable. The best attachment locations have positive attachment masses so that they are feasible and low sensitivities for all of the parameters considered.

The theoretical approach has been illustrated by experimental tests varying the base excitation frequency and the attachment location. The experiments varying the base excitation frequency showed good agreement between the theoretical and experimental effects of mistuning of the base excitation frequency with the real and theoretical nodes occurring within 2% of the same base excitation frequency. The tests of varied attachment locations also closely follow the behavior of the theoretical system. Furthermore, both sets of tests showed that for small deviations in the system parameters the amplitude increases significantly illustrating the importance of the sensitivity analysis. The experimental tests show that the procedure can be used to control vibrations in a real system that is lightly damped.

Acknowledgments

This material is based upon work supported by the National Science Foundation under Grant No. NSF-CMMI-1663376. This support is greatly appreciated.

References

[1] H. Frahm, Device for damping vibrations of bodies, US Patent 989,958, 1911.

[2] J. P. Den Hartog, Mechanical Vibration, Dover, 1985.

[3] J. E. Brock, A note on the damped vibration absorber, Transactions of the ASME, Journal of Applied Mechanics 13 (4) (1946) A–284.

[4] G. B. Warburton, Optimum absorber parameters for various combinations of response and excitation parameters, Earthquake Engineering & Structural Dynamics 10 (3) (1982) 381–401, doi:10.1002/eqe.4290100304.

[5] J. Q. Sun, M. R. Jolly, M. A. Norris, Passive, adaptive and active tuned vibration absorbers—a survey, Journal of Vibration and Acoustics 117 (B) (1995) 234–242, doi:10.1115/1.2838668.

[6] G. B. Warburton, E. O. Ayorinde, Optimum absorber parameters for simple systems, Earthquake Engineering and Structural Dynamics 8 (3) (1980) 197–217, doi:10.1002/eqe.4290080302.

[7] A. S. Joshi, R. S. Jangid, Optimum parameters of multiple tuned mass dampers for base-excited damped systems, Journal of Sound and Vibration 202 (5) (1997) 657–667, doi:10.1006/jsvi.1996.0859.

[8] H.-C. Tsai, G.-C. Lin, Optimum tuned-mass dampers for minimizing steady-state response of support-excited and damped systems, Earthquake Engineering and Structural Dynamics 22 (11) (1993) 957–973, doi:10.1002/eqe.4290221104.

[9] D. Young, Theory of dynamic vibration absorbers for beams, in: Proceedings of the First U.S. National Congress on Applied Mechanics, 1952.

[10] Y. Cheung, W. Wong, H_∞ and H_2 optimizations of a dynamic vibration absorber for suppressing vibrations in plates, Journal of Sound and Vibration 320 (1) (2009) 29–42, doi:10.1016/j.jsv.2008.07.024.

[11] R. G. Jacquot, Optimal dynamic vibration absorbers for general beam systems, Journal of Sound and Vibration 60 (4) (1978) 535–542, doi:10.1016/S0022-460X(78)80090-X.

[12] J. Dayou, Fixed-points theory for global vibration control using vibration neutralizer, Journal of Sound and Vibration 292 (3-5) (2006) 765–776, doi:10.1016/j.jsv.2005.08.032.

[13] P. D. Cha, Specifying nodes at multiple locations for any normal mode of a linear elastic structure, Journal of Sound and Vibration 250 (5) (2002) 923–934, doi:10.1006/jsvi.2001.3964.

[14] P. D. Cha, Imposing nodes at arbitrary locations for general elastic structures during harmonic excitations, Journal of Sound and Vibration 272 (3-5) (2004) 853–868, doi:10.1016/S0022-460X(03)00495-4.

[15] P. D. Cha, Enforcing nodes at required locations in a harmonically excited structure using simple oscillators, Journal of Sound and Vibration 279 (3-5) (2005) 799–816, doi:10.1016/j.jsv.2003.11.067.

[16] P. D. Cha, J. M. Rinker, Enforcing nodes to suppress vibration along a harmonically forced damped Euler-Bernoulli beam, Journal of Vibration and Acoustics 134 (5) (2012) 051010, doi:10.1115/1.4006375.

[17] P. D. Cha, X. Zhou, Imposing points of zero displacements and zero slopes along any linear structure during harmonic excitations, Journal of Sound and Vibration 297 (1-2) (2006) 55–71, doi:10.1016/j.jsv.2006.03.032.

[18] P. D. Cha, M. Chan, Mitigating vibration along an arbitrarily supported elastic structure using multiple two-degree-of-freedom oscillators, Journal of Vibration and Acoustics 131 (3) (2009) 031008, doi:10.1115/1.3085891.

[19] P. D. Cha, K. Buyco, An efficient method for tuning oscillator parameters in order to impose nodes on a linear structure excited by multiple harmonics, Journal of Vibration and Acoustics 137 (3) (2015) 031018, doi:10.1115/1.4029612.

[20] W. O. Wong, S. L. Tang, Y. L. Cheung, L. Cheng, Design of a dynamic vibration absorber for vibration isolation of beams under point or distributed loading, Journal of Sound and Vibration 301 (3-5) (2007) 898–908, doi:10.1016/j.jsv.2006.10.028.

[21] J. Rinker, Tuning TMDs to Fix Floors in MDOF Shear Buildings, in: Topics in Dynamics of Civil Structures, Volume 4, Springer, 55–59, doi:10.1007/978-1-4614-6555-3_7, 2013.

[22] P. W. Anderson, Absence of diffusion in certain random lattices, Physical Review 109 (1958) 1492–1505, doi:10.1103/PhysRev.109.1492.

[23] C. H. Hodges, Confinement of vibration by structural irregularity, Journal of Sound and Vibration 82 (3) (1982) 411–424, doi:10.1016/S0022-460X(82)80022-9.

[24] R. A. Ibrahim, Structural dynamics with parameter uncertainties, ASME Applied Mechanics Review 40 (3) (1987) 309–328, doi:10.1115/1.3149532.

[25] C. Pierre, D. M. Tang, E. H. Dowell, Localized vibrations of disordered multispan beams – Theory and experiment, AIAA Journal 25 (9) (1987) 1249–1257, doi:10.2514/3.9774.

[26] M. Foda, B. Albassam, Vibration confinement in a general beam structure during harmonic excitations, Journal of Sound and Vibration 295 (3) (2006) 491–517, doi:10.1016/j.jsv.2005.12.057.

[27] C. Pierre, E. H. Dowell, Localization of vibrations by structural irregularity, Journal of Sound and Vibration 114 (3) (1987) 549–564, doi:10.1016/S0022-460X(87)80023-8.

[28] P. D. Cha, C. Pierre, Vibration Localization by Disorder in Assemblies of Monocoupled, Multimode Component Systems, ASME Journal of Applied Mechanics 58 (4) (1991) 1072–1081, doi:10.1115/1.2897684.